The 9th European Congress on Computational Methods in Applied Sciences and Engineering
ECCOMAS Congress 2024
3–7 June 2024, Lisboa, Portugal

ON THE CONDITIONS FOR A STABLE PROJECTION METHOD ON COLLOCATED UNSTRUCTURED GRIDS

D. SANTOS, J. A. HOPMAN, C.D. PÉREZ-SEGARRA AND F.X. TRIAS

Heat and Mass Transfer Technological Center (CTTC)
Technical University of Catalonia
C/Colom, 11, Edifici TR4, 08222, Terrassa, Spain
e-mail:{daniel.santos.serrano, jannes.hopman, cdavid.perez.segarra, francesc.xavier.trias}
@upc.edu

Key words: FVM, Projection-methods, Symmetry-preserving, CFD, FSM, PISO

Summary. In this work, the conditions for a projection method, such as FSM or PISO, to be unconditionally stable are discussed for staggered and collocated configurations. In this regard, energy stability is guaranteed by preserving the underlying symmetries of the differential operators, assuming a suitable time integration, for staggered configurations. However, if a wide-stencil Laplacian is used in collocated arrangements, the checkerboard problem arises. For this reason, a compact Laplacian is usually preferred over the wide-stencil Laplacian. This choice avoids the checkerboard problem, but, on the other side, it introduces a new term in the kinetic energy equation that can introduce energy to the system. The conditions for this term to be non-positive are determined in this work.

1 INTRODUCTION

The Navier-Stokes equations for Newtonian, incompressible flows in dimensionless primitive variables read:

$$\frac{\partial \mathbf{u}}{\partial t} + \nabla \cdot (\mathbf{u} \otimes \mathbf{u}) = \frac{1}{Re}\Delta \mathbf{u} - \nabla p, \tag{1a}$$

$$\nabla \cdot \mathbf{u} = 0, \tag{1b}$$

where Re is the dimensionless Reynolds number. A fully-conservative finite-volume discretization, respecting the underlying symmetries of the continuous differential operators at a discrete level for collocated unstructured meshes, was first introduced in [1]. Assuming there are n control volumes and m faces:

$$\Omega \frac{d\mathbf{u}_c}{dt} + \mathsf{C}(\mathbf{u}_s)\,\mathbf{u}_c + \mathsf{D}\mathbf{u}_c + \Omega \mathsf{G}_c \mathbf{p}_c = \mathbf{0}_c, \tag{2a}$$

$$\mathsf{M}\mathbf{u}_s = \mathbf{0}_c, \tag{2b}$$

where $\mathbf{p}_c = (p_1, p_2, \ldots, p_n)^T \in \mathbb{R}^n$ and $\mathbf{u}_c \in \mathbb{R}^{3n}$ are the cell-centered pressure and collocated velocity fields, respectively. The cell-centered variables are marked with the subindex c, while the subindex s indicates that the variables are staggered at the faces. Mass conservation within each control volume is verified by defining a velocity field at the faces $\mathbf{u}_s =$

$\Big((u_s)_1,(u_s)_2,(u_s)_3,\ldots,(u_s)_m\Big)^T \in \mathbb{R}^m$. Variables defined at cells and at faces are related by using an interpolator from cells to faces $\Gamma_{c\to s} \in \mathbb{R}^{m\times 3n}$:

$$\mathbf{u}_s \equiv \Gamma_{c\to s}\mathbf{u}_c. \tag{3}$$

The matrices $\Omega \in \mathbb{R}^{3n\times 3n}$, $\mathsf{C}(\mathbf{u}_s) \in \mathbb{R}^{3n\times 3n}$ and $\mathsf{D} \in \mathbb{R}^{3n\times 3n}$ are block-diagonal matrices constructed using the Kronecker product:

$$\Omega = \mathsf{I}_3 \otimes \Omega_c, \quad \mathsf{C}(\mathbf{u}_s) = \mathsf{I}_3 \otimes \mathsf{C}_c(\mathbf{u}_s), \quad \mathsf{D} = \mathsf{I}_3 \otimes \mathsf{D}_c, \tag{4}$$

where $\mathsf{I}_3 \in \mathbb{R}^{3\times 3}$ is the identity matrix and $\Omega_c \in \mathbb{R}^{n\times n}$ is a diagonal matrix containing the cell-centered volumes. $\mathsf{C}_c(\mathbf{u}_s) \in \mathbb{R}^{n\times n}$ and $\mathsf{D}_c \in \mathbb{R}^{n\times n}$ are the cell-centered convective and diffusive operators for a discrete scalar field, respectively. Finally, $\mathsf{G}_c \in \mathbb{R}^{3n\times n}$ is the discrete gradient operator, and $\mathsf{M} \in \mathbb{R}^{n\times m}$ is the face-to-center discrete divergence operator matrix.

The 3−dimensional interpolator from cells to faces $\Gamma_{c\to s}$ is constructed by using the Kronecker product to create a 3−dimensional interpolator from the scalar one and projecting the interpolated quantities with the face-normal vectors:

$$\Gamma_{c\to s} = N(\mathsf{I}_3 \otimes \Pi_{c\to s}), \tag{5}$$

where $\Pi_{c\to s} \in \mathbb{R}^{m\times n}$ is the scalar cell-to-face interpolator, and $N = (N_{s,x}N_{s,y}N_{s,z}) \in \mathbb{R}^{3m\times m}$, where $N_{s,i} \in \mathbb{R}^{m\times m}$ is a diagonal matrix containing the x_i spatial components of the face normal vectors.

This formulation only requires five operators: the cell-centered and staggered control volumes, Ω_c and Ω_s, respectively, and the face normal vectors N (geometrical operators given by the chosen mesh), the scalar cell-to-face interpolation operator $\Pi_{c\to s}$, and the cell-to-face divergence operator M. This simplicity improves the portability of a code developed within this framework, as demonstrated in [2].

1.1 GLOBAL DISCRETE KINETIC ENERGY

Defining the discrete inner-product following [3];

$$< \mathbf{v}_c, \mathbf{u}_c >= \mathbf{v}_c^*\Omega\mathbf{u}_c, \tag{6}$$

the global discrete kinetic energy is computed by $||\mathbf{u}_c||^2 \equiv \mathbf{u}_c^*\Omega\mathbf{u}_c$ and its temporal evolution equation can be obtained by left-multiplying Eq.(2a) by $\mathbf{u}_c^*$, summing the resulting expression with its transpose and applying the chain rule:

$$\begin{aligned}\frac{d}{dt}||\mathbf{u}_c||^2 &= -\mathbf{u}_c^*\left(\mathsf{C}(\mathbf{u}_s) + \mathsf{C}^*(\mathbf{u}_s)\right)\mathbf{u}_c - \mathbf{u}_c^*\left(\mathsf{D}+\mathsf{D}^*\right)\mathbf{u}_c \\ &\quad -\mathbf{u}_c^*\Omega\mathsf{G}_c\mathbf{p}_c - \mathbf{p}_c^*\mathsf{G}_c^*\Omega^*\mathbf{u}_c.\end{aligned} \tag{7}$$

In absence of diffusion ($\mathsf{D} = 0$), the global kinetic energy $||\mathbf{u}_c||^2$ is conserved if the convective and pressure terms vanish for any:

$$\mathsf{C}(\mathbf{u}_s) = -\mathsf{C}(\mathbf{u}_s)^T, \tag{8a}$$

$$-(\Omega\mathsf{G}_c)^T = \mathsf{M}\Gamma_{c\to s}, \tag{8b}$$

thus relating the gradient operator with the divergence operator and assuming the convective operator to be skew-symmetric. The pressure term vanishes if, for any $\mathbf{u}_c$, $\mathsf{M}\Gamma_{c\to s}\mathbf{u}_c = \mathbf{0}_c$, that is, by using a wide-stencil Laplacian $\mathsf{L}_c = \mathsf{M}_c\mathsf{G}_c$. However, the well-known checkerboard problem is found with this approach. Alternatively, the use of a compact Laplacian $\mathsf{L} = \mathsf{MG}$ will be discussed in this work. Note that this problem is not encountered in staggered configurations, where respecting the symmetry of the gradient and the divergence is enough because $\mathsf{M}\mathbf{u}_s = \mathbf{0}_c$.

2 AN UNCONDITIONALLY STABLE PISO ALGORITHM

If explicit or implicit time integration is assumed, the spatially discrete momentum equation (2a) can be expressed in the following manner:

$$\mathbf{S}\mathbf{u}_c = \mathbf{r} - \mathsf{G}_c\mathbf{p}_c, \tag{9}$$

where the matrix $\mathbf{S} \in \mathbb{R}^{3n\times 3n}$ is obtained from the application of a discretization method like the Finite Volume Method. The vector $\mathbf{r} \in \mathbb{R}^{3n\times 1}$ holds all the explicit terms except for the pressure gradient. Once the discretization process is chosen, all the coefficients are already known.

When the pressure gradient is regarded as an explicit source, and the velocity is solved, the momentum predictor at time step $n+1$ is obtained:

$$\mathbf{u}_c^* = \mathbf{S}^{-1}\mathbf{r}^n - \mathbf{S}^{-1}\mathsf{G}_c\mathbf{p}_c^n. \tag{10}$$

A corrector step must be performed to ensure that the velocity satisfies the continuity equation. A diagonal matrix $\mathbf{A}$ (which will be easily invertible) is obtained by extracting the diagonal coefficients of $\mathbf{S}$, and the off-diagonal coefficients will be kept in a matrix $\mathbf{H}'$. Then, assuming that the diagonal matrix acts on a new corrected velocity $\mathbf{u}_c^{**}$ while the off-diagonal part acts on the predictor velocity $\mathbf{u}_c^*$, a divergence-free velocity is obtained.

The final algorithm reads [4]:

$$\begin{aligned}
\mathbf{u}_c^* &= \mathbf{S}^{-1}\mathbf{r} - \mathbf{S}^{-1}\mathsf{G}_c\mathbf{p}_c, && \text{(11a)}\\
\mathsf{M}\tilde{\mathbf{A}}^{-1}\mathsf{G}\mathbf{p}_c^* &= \mathsf{M}\Gamma_{c\to s}\mathbf{A}^{-1}(\mathbf{r} - \mathbf{H}'\mathbf{u}_c^*) \longrightarrow \mathbf{p}_c^*, && \text{(11b)}\\
\mathbf{u}_c^{**} &= \mathbf{A}^{-1}(\mathbf{r} - \mathbf{H}'\mathbf{u}_c^*) - \mathbf{A}^{-1}\mathsf{G}_c\mathbf{p}_c^*, && \text{(11c)}\\
\mathbf{u}_s^{**} &= \Gamma_{c\to s}\mathbf{A}^{-1}(\mathbf{r} - \mathbf{H}'\mathbf{u}_c^*) - \tilde{\mathbf{A}}^{-1}\mathsf{G}\mathbf{p}_c^*, && \text{(11d)}
\end{aligned}$$

where $\tilde{\mathbf{A}}^{-1} = diag(\Pi_{c\to s} vec(\mathbf{A}_c^{-1}))$ and $\mathbf{A} = I_3 \otimes \mathbf{A}_c$ (the matrix $\mathbf{A}$ has three equal (diagonal) blocks). The PISO algorithm iterates through the corrector steps until the desired level of convergence is achieved. In this context, the compact Laplacian operator, L, is assumed to mitigate checkerboard problems.

2.1 ARTIFICIAL KINETIC ENERGY ADDED BY THE COMPACT LAPLACIAN ASSUMPTION

Applying the face-to-cell $\mathsf{M}_c = \mathsf{M}\Gamma_{c\to s}$ divergence operator to Eq.(11c) (apart from the predictor velocity mark, let us drop the superscript for simplicity):

$$\mathsf{M}_c\mathbf{u}_c = \mathsf{M}_c\mathbf{A}^{-1}(\mathbf{r} - \mathbf{H}'\mathbf{u}_c^*) - \mathsf{M}_c\mathbf{A}^{-1}\mathsf{G}_c\mathbf{p}_c \tag{12}$$

Subtracting the divergence M of Eq. (11d) from Eq. (12):

$$\mathsf{M}_c\mathbf{u}_c = \mathsf{M}\tilde{\mathbf{A}}^{-1}\mathsf{G}\mathbf{p}_c - \mathsf{M}_c\mathbf{A}^{-1}\mathsf{G}_c\mathbf{p}_c. \tag{13}$$

Now, using Eq.(8b), the pressure gradient term in Eq.(7) can be rewritten as:

$$-\mathbf{p}_c^T\mathsf{G}_c^T\Omega^T\mathbf{u}_c = \mathbf{p}_c^T\mathsf{M}_c\mathbf{u}_c. \tag{14}$$

Finally, plugging Eq.(13) into Eq.(14):

$$\mathbf{p}_c^T\mathsf{M}_c\mathbf{u}_c = \mathbf{p}_c^T(\mathsf{M}\tilde{\mathbf{A}}^{-1}\mathsf{G} - \mathsf{M}_c\mathbf{A}^{-1}\mathsf{G}_c)\mathbf{p}_c. \tag{15}$$

This term would be the artificial kinetic energy the pressure gradient adds when the compact Laplacian is used. In the particular case of explicit schemes, $\mathbf{A}^{-1} = \Delta t \cdot \mathsf{I}_{3n\times 3n}$, so:

$$\mathbf{p}_c^T(\mathsf{M}\mathsf{G} - \mathsf{M}_c\mathsf{G}_c)\mathbf{p}_c\Delta t = \mathbf{p}_c^T(\mathsf{L} - \mathsf{L}_c)\mathbf{p}_c\Delta t. \tag{16}$$

Defining, for both explicit and implicit time-integration, the wide-stencil Laplacian and the compact Laplacian as $\mathsf{L}_c = \mathsf{M}_c\mathbf{A}^{-1}\mathsf{G}_c$ and $\mathsf{L} = \mathsf{M}\tilde{\mathbf{A}}^{-1}\mathsf{G}$, respectively, the (artificial) contribution to the kinetic energy will be:

$$\mathbf{p}_c^T(\mathsf{M}\tilde{\mathbf{A}}^{-1}\mathsf{G} - \mathsf{M}_c\mathbf{A}^{-1}\mathsf{G}_c)\mathbf{p}_c = \mathbf{p}_c^T(\mathsf{L} - \mathsf{L}_c)\mathbf{p}_c. \tag{17}$$

Both L and L_c are symmetric and semi-negative definite. This term's contribution should be strictly non-positive (it damps kinetic energy) and ideally as small as possible in absolute value.

It should be noted that any projection method that results in equations being solved this way will face the same issue. For instance, the classical Fractional Step Method [5], which resembles the PISO algorithm but lacks a predictor step and corrector iterations, will encounter this problem.

2.2 RELATION BETWEEN $\mathsf{L} - \mathsf{L}_c$ AND THE INTERPOLATOR OPERATOR

To maintain a non-positive contribution to the global kinetic energy, it is required $\mathsf{L} - \mathsf{L}_c$ to be semi-negative definite (see Eq. (17)). This matrix reads,

$$\begin{aligned}\mathsf{L} - \mathsf{L}_c &= -\mathsf{M}\tilde{\mathbf{A}}^{-1}\Omega_s^{-1}\mathsf{M}^T + \mathsf{M}\Gamma_{c\to s}\mathbf{A}^{-1}\Omega^{-1}\Gamma_{c\to s}^T\mathsf{M}^T \\ &= -\mathsf{M}(\tilde{\mathbf{A}}^{-1}\Omega_s^{-1} - \Gamma_{c\to s}\mathbf{A}^{-1}\Omega^{-1}\Gamma_{c\to s}^T)\mathsf{M}^T.\end{aligned} \tag{18}$$

The next step consists of removing both divergence operators from the extremes. According to [6] (Theorem 4.2.1, page 141), the definiteness of $-\mathsf{M}(\tilde{\mathbf{A}}^{-1}\Omega_s^{-1} - \Gamma_{c\to s}\mathbf{A}^{-1}\Omega^{-1}\Gamma_{c\to s}^T)\mathsf{M}^T$ is given by the definiteness of $\tilde{\mathbf{A}}^{-1}\Omega_s^{-1} - \Gamma_{c\to s}\mathbf{A}^{-1}\Omega^{-1}\Gamma_{c\to s}^T$, so, requiring $\mathsf{L}-\mathsf{L}_c$ to be semi-negative definite is equivalent to require $\tilde{\mathbf{A}}^{-1}\Omega_s^{-1} - \Gamma_{c\to s}\mathbf{A}^{-1}\Omega^{-1}\Gamma_{c\to s}^T$ being semi-positive definite. Then, multiplying each side of the expression by $\tilde{\mathbf{A}}^{\frac{1}{2}}\Omega_s^{\frac{1}{2}}$ (note that both Ω_s and $\tilde{\mathbf{A}}$ are diagonal with positive components) we obtain:

$$\mathsf{I} - \tilde{\mathbf{A}}^{\frac{1}{2}}\Omega_s^{\frac{1}{2}}\Gamma_{c\to s}\mathbf{A}^{-1}\Omega^{-1}\Gamma_{c\to s}^T\Omega_s^{\frac{1}{2}}\tilde{\mathbf{A}}^{\frac{1}{2}}. \tag{19}$$

If $\mathsf{B} = \tilde{\mathbf{A}}^{\frac{1}{2}}\Omega_s^{\frac{1}{2}}\Gamma_{c\to s}\mathbf{A}^{-1}\Omega^{-1}\Gamma_{c\to s}^T\Omega_s^{\frac{1}{2}}\tilde{\mathbf{A}}^{\frac{1}{2}}$, we require $\rho(\mathsf{B}) \leq 1$, being $\rho(\cdot)$ the spectral radius (observe that B is semi-positive definite).

Defining $\mathsf{E} = \mathbf{A}^{-\frac{1}{2}}\Omega^{-\frac{1}{2}}\Gamma_{c\to s}^T\Omega_s^{\frac{1}{2}}\tilde{\mathbf{A}}^{\frac{1}{2}}$, the previous matrix can be constructed as $\mathsf{B} = \mathsf{E}^T\mathsf{E}$. Another matrix $\mathsf{C} = \mathsf{E}\mathsf{E}^T$ switching the transpose operator can be constructed.

Observe that, if λ is a non-zero eigenvalue of $\mathsf{E}^T\mathsf{E}$:

$$\mathsf{E}^T\mathsf{E}\mathbf{w} = \lambda\mathbf{w} \implies (\mathsf{E}\mathsf{E}^T)\mathsf{E}\mathbf{w} = \lambda\mathsf{E}\mathbf{w}, \tag{20}$$

so $eigen(\mathsf{E}^T\mathsf{E}) = eigen(\mathsf{E}\mathsf{E}^T)$ except for $\lambda = 0$ (and its multiplicity) eigenvalue. So,

$$\rho(\mathsf{C}) = \rho(\mathsf{B}) \Rightarrow (\rho(\mathsf{B}) \leq 1 \Leftrightarrow \rho(\mathsf{C}) \leq 1). \tag{21}$$

Then, we require $\mathsf{I} - \mathbf{A}^{-\frac{1}{2}}\Omega^{-\frac{1}{2}}\Gamma_{c\to s}^T\tilde{\mathbf{A}}\Omega_s\Gamma_{c\to s}\Omega^{-\frac{1}{2}}\mathbf{A}^{-\frac{1}{2}}$ to be semi-positive definite. Finally, multiplying the previous expression by $\mathbf{A}^{\frac{1}{2}}\Omega^{\frac{1}{2}}$ at each side:

$$\mathbf{A}\Omega - \Gamma_{c\to s}^T\tilde{\mathbf{A}}\Omega_s\Gamma_{c\to s}. \tag{22}$$

Summarizing, it has been shown that $\mathsf{L} - \mathsf{L}_c$ being semi-negative definite is equivalent to $\mathbf{A}\Omega - \Gamma_{c\to s}^T\tilde{\mathbf{A}}\Omega_s\Gamma_{c\to s}$ being semi-positive definite.

3 GEOMETRICAL CONDITIONS OF A PROJECTION METHOD TO BE UNCONDITIONALLY STABLE

Let us assume a general 2D or 3D mesh is constructed such that each control volume satisfies:

- **1.** $V_k = \sum_f \tilde{V}_{k,f} n_{i,f}^2, \quad \forall k \in \{1, ..., n\}, \quad i \in \{x, y, z\},$
- **2.** $\sum_f \tilde{V}_{k,f} n_{i,f} n_{j,f} \leq 0, \forall k \in \{1, ..., n\}, \quad i, j \in \{x, y, z\}, \quad i \neq j,$

where V_k is the volume of the control volume, $n_{i,f}$ are the components of the normal vector to the face f, and $\tilde{V}_{k,f}$ is constructed multiplying the distance between the cell center and the face by the face area (see Fig.3). Then, $\mathsf{L} - \mathsf{L}_c$ is semi-negative definite for the provided discretization if the chosen interpolator is the volume-weighted one (this choice is unique for both $\mathsf{G}_c\mathbf{p}_c$ in the velocity correction equation and in the computation of $\tilde{\mathbf{A}}$). The converse is also true. The proof of this fact is cumbersome and consists of proving when Eq.(22) is semi-positive definite. It was developed by the author and can be found in [7].

The volume-weighted interpolator [8] can be computed in any mesh as follows:

$$\Pi_{c\to s} = \Delta_s^{-1}\Delta_{sc}^T, \tag{23}$$

where $\Delta_s \in \mathbb{R}^{m\times m}$ is a diagonal matrix containing the projected distances between two adjacent control volumes, and $\Delta_{sc} \in \mathbb{R}^{n\times m}$ is a matrix containing the projected distances between an adjacent cell node and its corresponding face. Fig.3 shows a representation of these distances.

Some consequences of the previous theorem are the following ones:

- Even highly distorted square or cubic meshes are stable when using the volume-weighted interpolator.
- Triangular meshes are stable when placing the cell node at the circumcenter. However, this restricts how to construct them because the circumcenter lies outside obtuse-angled triangles.
- If the geometrical conditions are not met, it is possible for $\mathsf{L} - \mathsf{L}_c$ to be neither positive nor negative definite, so it may or may not introduce energy. Typically, energy is not introduced for low-aspect ratio meshes, even when using other interpolators.

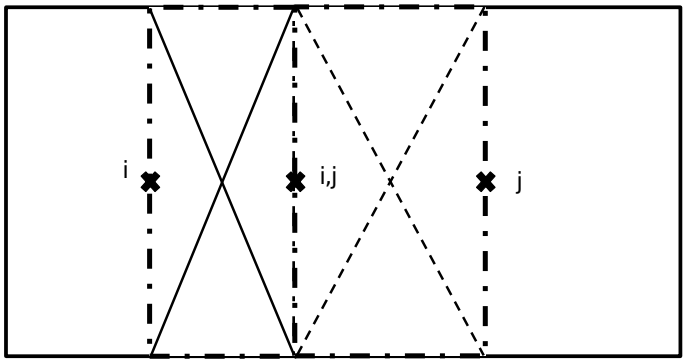

Figure 1: Control volume i and control volume j, sharing a common face $f(i,j)$. The volume crossed with a continuous line is the quantity of staggered volume associated with control volume i, $\tilde{V}_{i,f(i,j)}$. The volume crossed with a discontinuous line is the quantity of staggered volume associated with control volume j, $\tilde{V}_{j,f(i,j)}$.

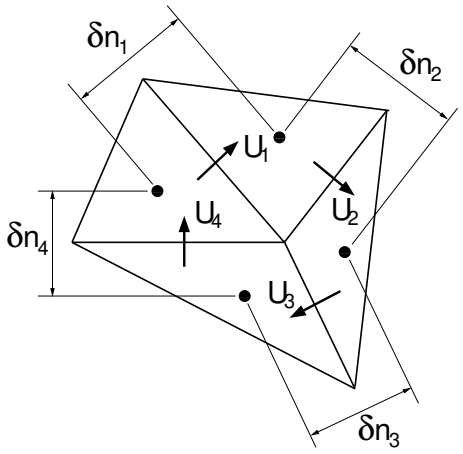

Figure 2: δn_i are the components of Δ_s, while the components of Δ_{sc} would be calculated similarly, taking the distance between a control volume and their corresponding face centers.

4 TEST CASE: TURBULENT CHANNEL FLOW AT $Re_\tau = 395$

This section evaluates the method's robustness and accuracy through simulations of a channel flow at $Re_\tau = 395$, using different meshes. The simulation domain selected is in line with the work of Moser et al. [9] and is $2\pi \times 2 \times \pi$. All meshes maintain a y^+ value of approximately 1. In these simulations, a volume-weighted interpolation is used, and it is compared with other interpolations such as a midpoint interpolation (with interpolation coefficients of $\frac{1}{2}$) and a linear interpolation.

4.1 ACCURACY OF THE INTERPOLATOR ON HIGH-QUALITY MESHES

The mesh illustrated in Fig. 3 was selected to study the accuracy. It features stretching along the y-direction. In Fig. 4, the normalized mean velocity (in wall units) and the $< u'v' >$ component of the Reynolds stress tensor are shown. The results are compared against the DNS data from Moser et al. [9]. The results show remarkable similarity between all three

interpolators. This was expected because all three interpolators converge to the same (midpoint) interpolator for regular Cartesian meshes. Furthermore, when the stretching ratio is relatively small, the mesh is virtually regular and locally Cartesian.

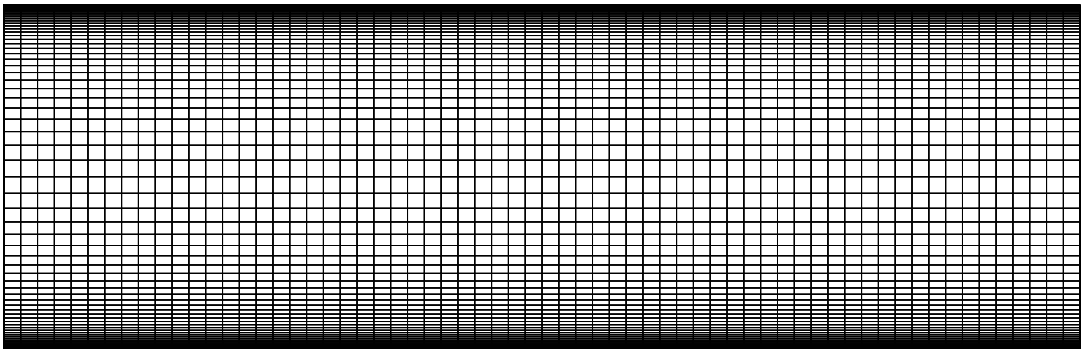

Figure 3: 64x64x64 mesh used to test our method with different interpolators.

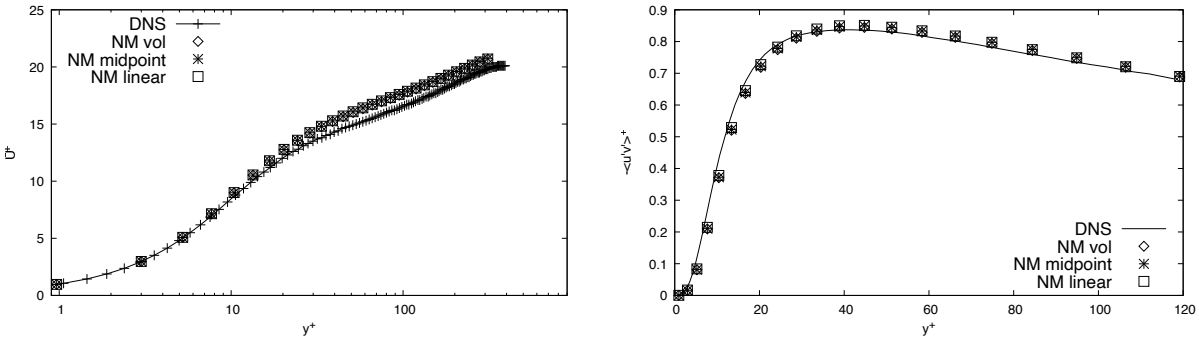

Figure 4: Normalised mean velocity profile in wall units for channel flow at $Re_\tau = 395$ and normalized turbulent shear stress profile $- < u'v' >$ in wall units at $Re_\tau = 395$.

4.2 ROBUSTNESS IN DISTORTED MESHES

The mesh shown in Fig. 5 is chosen to assess the method's robustness. Long control volumes are present in the center, and the mesh is stretched towards both ends. As expected for this type of mesh, the results are unsatisfactory, even from a qualitative standpoint (turbulence is not triggered, and the central control volumes filter out any eddy). Despite this, the only interpolation method that converges to a solution is the volume-weighted interpolation, while the others were unstable.

In Fig. 6, you can see a mesh with less distortion, featuring a maximum aspect ratio between adjacent control volumes of 5, which is typical in many cases. The linear interpolation does not cause turbulence even with this moderately distorted mesh. On the other hand, the results from the midpoint and volume-weighted interpolations are pretty similar, as shown in Fig. 7 (results from linear interpolation are not shown due to their inaccuracy).

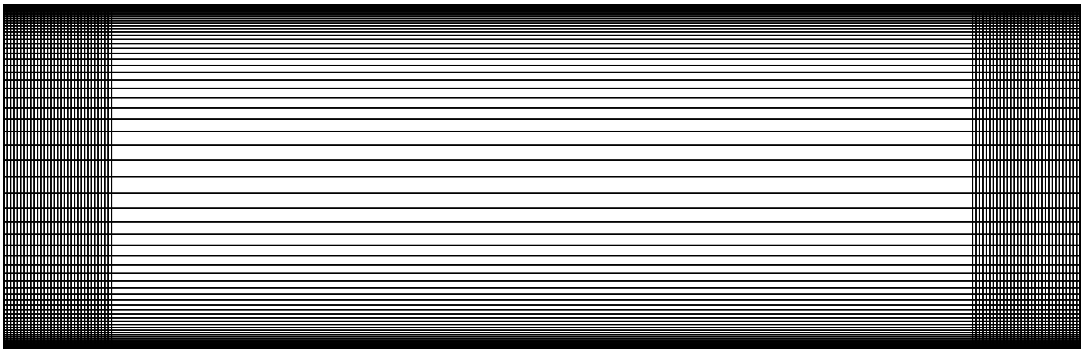

Figure 5: Highly distorted mesh used to test the method's robustness. The maximum aspect ratio between adjacent control volumes is 250.

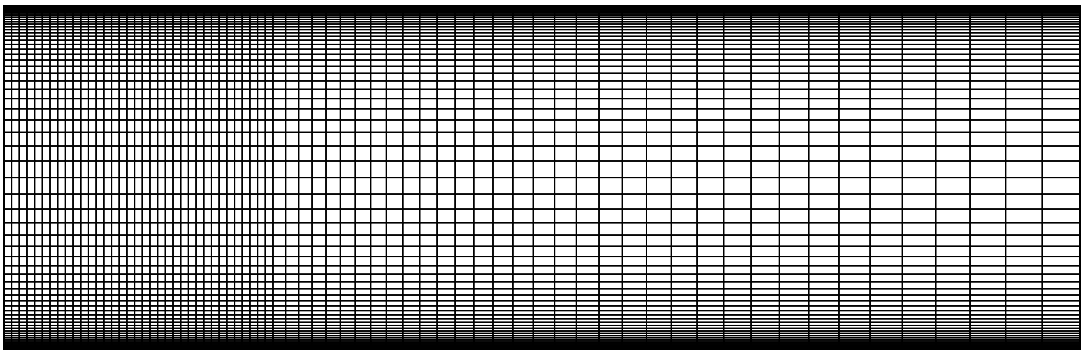

Figure 6: Mesh which starts growing the control volumes at 1/3 of total length. The maximum aspect ratio between adjacent control volumes is 5.

The results are not as precise as those achieved with the initial Cartesian mesh, as expected, but they are still acceptable. It might be unexpected that the midpoint and volume-weighted interpolators produce similar results, while the linear interpolation, despite converging, generates unsatisfactory results. It is expected to find a stretching point when the midpoint interpolation fails while the volume-weighted interpolation remains unconditionally stable.

5 CONCLUSIONS

In this work, the necessary and sufficient conditions for a projection method, such as FSM or PISO, to be unconditionally stable are established for both staggered and collocated arrangements. In this regard, energy stability is guaranteed by preserving the underlying symmetries of the differential operators, provided that appropriate time integration is utilized for staggered configurations. However, for collocated meshes, a wide-stencil Laplacian will lead to checkerboarding. To avoid that problem, a compact Laplacian is usually preferred. This choice introduces an artificial term in the kinetic energy equation that can introduce energy to the system. The conditions for this term to be non-positive, apart from respecting the underlying symmetries of the operators, were identified: it is required to use the volume-weighted interpolator for momentum quantities, and the mesh must satisfy some geometrical restrictions. These

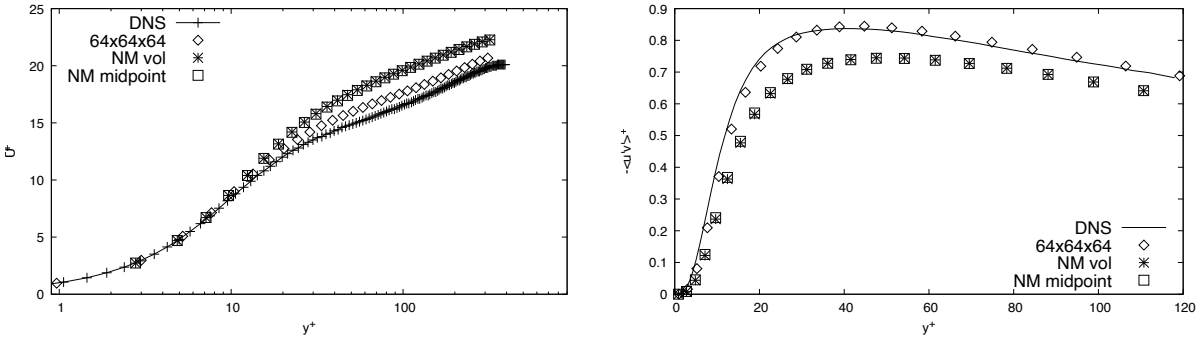

Figure 7: Normalised mean velocity profile in wall units for channel flow at $Re_\tau = 395$ and normalized turbulent shear stress profile $- < u'v' >$ in wall units at $Re_\tau = 395$.

geometrical restrictions are automatically satisfied by Hexahedral grids (such as cuboidal ones) and by triangular grids if the cell node is placed at the circumcenter. The method's robustness was tested with a turbulent channel flow at $Re_\tau = 395$. The volume-weighted interpolator, along with a midpoint and a linear interpolator, was tested using hexahedral meshes. The results were the same for low-distorted meshes, while the volume-weighted interpolator was the only one able to provide results for high-distorted ones.

AKNOWLEDGEMENTS

This work is supported by the SIMEX project (PID2022-142174OB-I00) of *Ministerio de Ciencia e Innovación* and the RETOtwin project (PDC2021-120970-I00) of *Ministerio de Economía y Competitividad*, Spain. D. Santos acknowledges a *FI AGAUR-Generalitat de Catalunya* fellowship (2022FI_B_00173), extended and financed by *Universitat Politècnica de Catalunya and Banc Santander*. J.A.H. is supported by the predoctoral grant FI 2023 (2023 FI_B1 00204) of the *Catalan Agency for Management of University and Research Grants (AGAUR)*.

REFERENCES

[1] Trias, F. X., Lehmkuhl, O., Oliva, A., Pérez-Segarra, C. D., and Verstappen, R. W. C. P. 2014. "Symmetry-preserving discretization of Navier-Stokes equations on collocated unstructured meshes." J Comput Phys, 258: 246–267. https://doi.org/10.1016/j.jcp.2013.10.031

[2] Álvarez, X., Gorobets A. and Trias F. X. 2021. "A hierarchical parallel implementation for heterogeneous computing. Application to algebra-based CFD simulations on hybrid supercomputers." Comput. Fluids, 214. https://doi.org/10.1016/j.compfluid.2020.104768

[3] Verstappen, R. W. C. P. and Veldman, A. E. P. 2003. "Symmetry-Preserving Discretization of Turbulent Flow." J Comput Phys, 187: 343–368. https://doi.org/10.1016/S0021-9991(03)00126-8

[4] Issa, R. I. 1986. "Solution of the implicitly discretized fluid flow equations by operator-splitting." J Comput Phys, 62: 40–65. https://doi.org/10.1016/0021-9991(86)90099-9

[5] Chorin, A. J. 1968. "Numerical Solution of the Navier-Stokes Equations." Math Comput, 22: 745–762. https://doi.org/10.2307/2004575

[6] Golub, G. H. and Van Loan C.E. 1996. "Matrix Computations, 3rd Edition". Edited by Johns Hopkins University Press. ISBN-10: 0801854148

[7] Santos, D., Hopman, J. A., Pérez-Segarra, C. D. and Trias, F. X. 2023. "On an Energy-Preserving Unconditionally Stable Projection Method on Collocated Unstructured Grids." Available at SSRN: https://ssrn.com/abstract=4788673 or http://dx.doi.org/10.2139/ssrn.4788673

[8] Santos D., Muela J., Valle N. and Trias F. X. 2021. "On the Interpolation Problem for the Poisson Equation on Collocated Meshes." In Proc. 14th WCCM-ECCOMAS Congress, Paris.

[9] Moser R., Kim, J. and Mansour, N. 1999. "Direct numerical simulation of turbulent channel flow up to $Re_\tau = 590$". Phys Fluids, 11-4: 943–945. https://doi.org/10.1063/1.869966